Applied Physics Letters ARTICLE pubs.aip.org/aip/apl

Elimination of reflection losses in gradient metasurface optical elements

Cite as: Appl. Phys. Lett. **124**, 031701 (2024); doi: 10.1063/5.0177947
Submitted: 13 October 2023 · Accepted: 2 January 2024 ·
Published Online: 17 January 2024

View Online Export Citation CrossMark

Mengdi Sun[1] and Pieter G. Kik[2,a)]

AFFILIATIONS

[1]CREOL, The College of Optics and Photonics, University of Central Florida, 4000 Central Florida Blvd., Orlando, Florida 32816, USA
[2]Physics Department, University of Central Florida, 4000 Central Florida Blvd., Orlando, Florida 32816, USA

[a)]Author to whom correspondence should be addressed: kik@creol.ucf.edu

ABSTRACT

Optical metasurfaces can achieve arbitrary wavefront control using subwavelength nanostructures, enabling imaging, sensing, and display applications using ultrathin structures. Metasurface optical elements that rely on propagation phase achieve this control using varying fill fractions of high refractive index materials, resulting in surface regions with significantly different effective refractive index. The intrinsic need for index variation makes it a non-trivial task to eliminate reflection losses across a complete optical element. Here, we investigate the optical performance of high-index metasurfaces, modified to suppress surface reflections. We demonstrate that a drastic reduction of surface reflections across an entire gradient metasurface is possible through the application of a single optimized anti-reflective layer with a thickness and refractive index that are substantially different from the traditionally expected values.

The advent of metasurface optics has led to a wide range of applications involving flat optical devices,[1–3] including active wavefront control,[4,5] sensing,[6–8] imaging,[9–11] nonlocal flat optics,[12] quantum technology,[13] and 3D displays.[14–16] Metasurface optical elements can approach or exceed the performance of traditional optical elements in certain scenarios. They offer unprecedented flexibility in optical functionality using compact structures that can be fabricated through standard 2D lithographic techniques. Despite the many appealing aspects of metasurface optical elements, their novel design introduces new challenges in optical systems. One interesting challenge in the use of gradient metasurface optics is the introduction of surface reflections that vary across the optical element. In imaging systems, even a small amount of reflection introduced by lenses can lead to notable visual artifacts in high-contrast images. In traditional optics, these issues are readily mitigated through the application of anti-reflective coatings (ARC) using well-established design rules. Such antireflective coatings are commonly applied in eyeglasses, microscope optics, and zoom lenses to suppress imaging artifacts originating from multiple surface reflections. However, as shown below, for gradient metasurfaces that operate based on spatial variation of propagation phase, the traditional design rules do not produce minimized reflection and cause significant spatial variation of reflection losses. Here, we introduce a methodology to achieve minimal reflection over a wide range of metasurface geometries.

A traditional thin-film ARC eliminates backreflection from a high-index optical element by introducing two reflecting interfaces, each producing a reflected field of equal amplitude, where one of the reflected fields incurs an additional phase delay. For the correct choice of ARC index and thickness, the reflected fields are of equal amplitude and in antiphase resulting in perfect destructive interference in the backward direction. Given a bulk optic with known index n_{sub} surrounded by air, the traditional ARC index n_{ARC} and thickness d_{ARC} achieve this condition by setting $n_{ARC} = \sqrt{n_{sub}}$ and $d_{ARC} = \lambda_0/4n_{ARC}$, respectively. However, as we demonstrate in the following, this traditional choice of ARC design cannot directly be applied to metasurface optical elements. Gradient metasurface optical elements typically make use of lateral patterning of a high-refractive index layer to achieve effective index gradients, allowing spatially varying propagation phase delays. As an example, Fig. 1(a) shows a region of an amorphous silicon-based metasurface lens, taken from Ref. 17, revealing strong local variation of the silicon fill fraction across the lens surface. The resulting spatial variation of the effective index represents the core challenge that is addressed in this manuscript: in order to achieve the lowest possible reflection, each region of the metasurface would require a region-specific ARC index and thickness, neither of which can easily be ensured using standard fabrication steps. In the present study, we first demonstrate this challenge quantitatively, followed by the introduction and in-depth analysis of a strategy that produces significantly reduced reflection losses across a wide range of fill fractions, and that is compatible with traditional device processing steps.

To demonstrate the challenge and its impact, Fig. 1(b) shows the reflectance at $\lambda_0 = 1550$ nm of a silicon-based metasurface for a wide range of fill fractions, calculated using rigorous coupled wave analysis (RCWA)[18] as implemented in RETICOLO.[19] The structure consists of an infinitely extended metasurface containing square silicon pillars ($n = 3.5$) in air with a width W placed on a square lattice with period $L = 200$ nm. The horizontal axis represents the Si areal fill fraction $f = (W/L)^2$. Without an ARC applied, regions with large fill fraction suffer from surface reflection losses as high as 30.9% (black curve). As the fill fraction is reduced, the effective index drops, which results in a drop of the reflection loss. To further reduce the reflection loss, a seemingly reasonable approach is to apply an ARC on the Si layer before patterning, using the traditional index choice and thickness. After patterning the metasurface, this produces the structure shown in the inset of Fig. 1(b). This approach produces a large drop in reflection for high fill fractions (red curve), but the reflection rapidly increases as the fill fraction is reduced. This intrinsic failure of the standard AR-coating approach when applied to gradient metasurfaces can be significantly mitigated, as will be shown below.

To illustrate the physical origin of the breakdown of the standard ARC approach on metasurfaces, we first consider an effective medium description for 1D metasurfaces. Figure 1(c) shows the calculated effective index of a deeply subwavelength grating for a material with index $n = 4$ as a function of fill fraction (orange line) under TE excitation. As the fill fraction of the high-index rods is reduced, the effective index $n_{eff,rods}$ drops gradually. At each fill fraction, the optimum AR coating index would be given by $n_{eff,opt} = \sqrt{n_{eff,rods}}$ as shown by the dashed blue line. However, interestingly when the high index layer is coated with a layer that has the traditional ARC index $n_{ARC} = \sqrt{n}$ (black solid line) before patterning, after patterning this produces a non-ideal $n_{eff,ARC}$ indicated by the solid blue line. Note that for all fill fractions $0 < f < 1$, the obtained effective index of the ARC region $n_{eff,ARC}$ is less than the ideal value, based on the analytical effective medium theory. To compensate for this effect, the 1D metasurface could be coated with a material that has a different index for each separate fill fraction, with an index n_{opt} that is higher for lower fill fractions (green line). In addition, for each region, there would be a unique optimum thickness (not

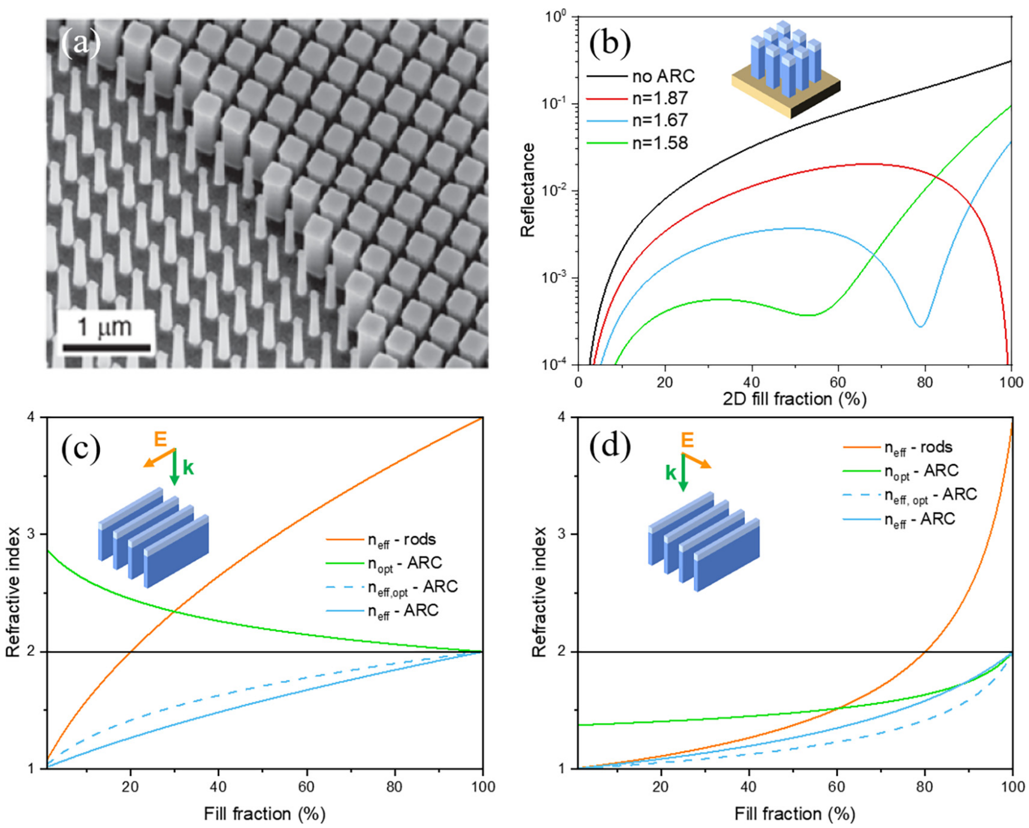

FIG. 1. (a) SEM image of a Si-based metasurface lens, reproduced with permission from Kamali *et al.*, Laser Photonics Rev. **10,** 1002–1008 (2016). Copyright 2016 Wiley-VCH GmbH.[17] (b) Calculated reflectance values for Si-based metasurfaces as a function of Si fill fraction without ARC (black line), with $n_{ARC} = 1.87$ (red line), $n_{ARC} = 1.67$ (blue line), and $n_{ARC} = 1.58$ (green line). (c) and (d) Effective index of rods made of a material with $n = 4$ (orange line) as a function of the fill fraction in 1D structures, the corresponding to traditional ARC refractive index choice $n = 2$ (black line), the resulting effective index of the ARC region (solid blue line), the desired effective index of the ARC region (dashed blue line), and the required index of the ARC material to achieve the ideal effective index (green line) at each fill fraction for TE and TM polarizations, respectively.

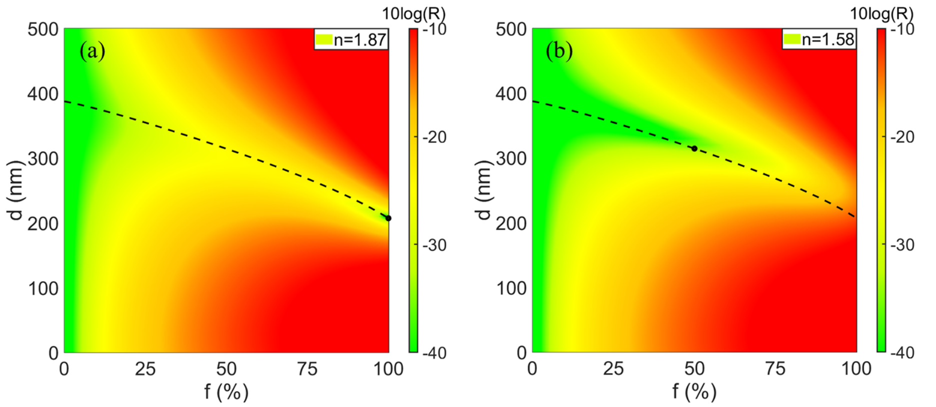

FIG. 2. Reflectance at $\lambda_0 = 1550$ nm of a Si metasurface with unit cell size of L = 200 nm as a function of Si areal fill fraction and ARC thickness for (a) an ARC material index of 1.87 and (b) an ARC material index of 1.58.

shown) given by $\lambda_0/4n_{eff,opt}$. This is not practical in real-word applications. For TM polarization [Fig. 1(d)], the fill fraction dependence is markedly different, but a similar challenge appears: the optimal ARC material index is different for each fill fraction used. These examples highlight that even in idealized 1D metasurfaces, applying a traditional ARC before patterning *intrinsically* leads to deviations of the ARC index from the optimum value for all fill fractions $0 < f < 1$. Unlike the case of traditional bulk optics, in metasurface optics, there exists no single ARC layer thickness and ARC index that can be applied before patterning to achieve ideal anti-reflective behavior.

As demonstrated above, no single ARC material deposited before metasurface patterning produces perfect AR behavior. In the following, we will show that improved choices can be made for both the refractive index of the ARC material and the thickness of the patterned ARC layer on an isotropic Si metasurface, leading to substantially improved performance. We consider a 2D metasurface intended for use at a wavelength of 1550 nm ($n_{Si} = 3.5$) with a square unit cell size of L = 200 nm. In order to identify improved antireflective behavior, Fig. 2(a) shows a contour graph of the calculated metasurface reflectance as a function of Si fill fraction and ARC layer thickness, with the ARC index set to the traditional value of $n_{ARC} = \sqrt{n_{Si}}$. The reflectance is shown on a log scale from 0.01% to 10%, with green regions indicating a reflectance below 0.1%. As expected, for low Si fill fractions, the reflectance is always low independent of the AR layer thickness, since in this region, the metasurface has a refractive index close to that of air. At the other end of the fill fraction range, for a Si fill fraction of 1, we see that a minimum reflection of ~0.01% is achieved close to $d_{ARC} = 207$ nm as indicated by the black dot on the contour graph, corresponding to the traditionally expected optimum thickness of $d_{ARC} = \lambda_0/4n_{ARC}$. However, for many intermediate Si fill fractions, the reflectance at this thickness exceeds 1%, corresponding to the data shown in Fig. 1(b) (red line).

In order to reduce the reflection for intermediate Si fill fractions f that are commonly used in metasurface lenses, we look for modified ARC index and thickness values that provide improved performance across a wide fill fraction range. As a starting point, we use an effective medium model[20] to estimate the index of a medium consisting of square pillars with dielectric function ε_r in air. This approach can be shown (see the supplementary material) to result in an effective relative permittivity given by

$$\varepsilon_{eff} = \left(1 - \sqrt{f}\right) + \frac{\sqrt{f}}{\left(1 - \sqrt{f}\right) + \sqrt{f}/\varepsilon_r}. \qquad (1)$$

This formula is most accurate for high-fill fraction subwavelength square gratings, but as demonstrated below provides a practical guideline for selecting an appropriate ARC material index and layer thickness. Based on the effective medium model, we estimate the effective index of the patterned Si region $n_{eff,Si}$ for any fill fraction. We then use the same effective medium model to find the ARC *material* index needed to achieve the corresponding optimum $n_{eff,ARC} = \sqrt{n_{eff,Si}}$. Finally, we use this optimal ARC index to determine the corresponding optimized ARC thickness given by $d_{ARC} = \lambda_0/4n_{eff,ARC}$. The black dashed line in Fig. 2(a) shows the thus estimated optimum ARC layer thickness for each areal fill fraction f.

Following the approach outlined above, we determine an optimized ARC material index and ARC thickness for a given fill fraction of choice, here $f = 0.5$, and subsequently evaluate the resulting reflectance across a wide fill factor range. At a fill fraction of $f = 0.5$, the effective medium model gives $n_{Si,eff} = 1.53$, which would require an $n_{eff,ARC}$ of 1.24 in order to achieve minimum reflection. To achieve this effective ARC index, the effective medium model predicts that we require a material with $n_{ARC} = 1.58$ and a corresponding optimum $d_{ARC} = 314$ nm. Figure 2(b) shows the calculated reflectance contour graph for this nontraditional ARC material index choice. For reference, the optimized thickness $d_{ARC} = 314$ nm for $f = 0.5$ is indicated by the black dot. Note that low reflection is indeed achieved near the calculated optimum thickness at a fill fraction of $f = 0.5$, showing good correspondence with the effective medium-based prediction. The resulting reflectance as a function of fill fraction for this *fixed* choice of n_{ARC} and d_{ARC} is included in Fig. 1(b) (green line). A reflection minimum is observed close to $f = 0.5$, and the reflectance is seen to be at least a factor 5 lower than obtained using the traditional approach (red line) for all fill fractions up to 73%. A similar curve optimized for a fill fraction of $f = 0.75$ is shown as the blue line. In this case, $R < 0.5\%$ can be achieved for a wide range of fill fractions spanning from 0% to 88%, whereas the traditional ARC parameter choices would lead to significantly larger reflectance across this same region. Note that this range of fill fractions includes common fill fractions used in gradient metasurfaces, since fill fractions close to zero and close to one are typically avoided due to the resulting need for impractically small features sizes.

To demonstrate the notable differences in geometry and as well as substantial performance differences between our approach and the traditional approach (i.e., applying a standard ARC before patterning), Figures 3(a)–3(d) show cross-sectional views of the time-averaged E-field magnitude above 2D Si-based metasurfaces when illuminated

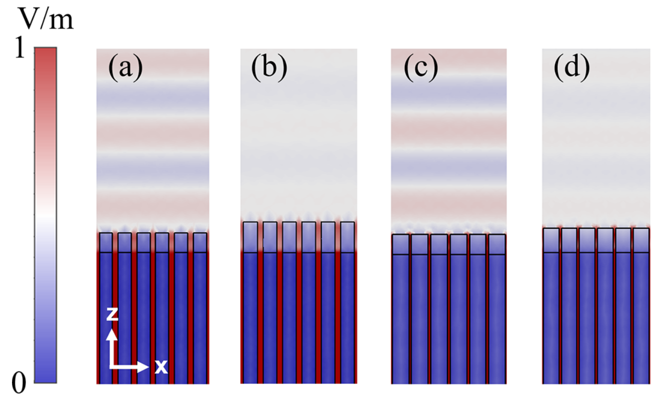

FIG. 3. Average electric field magnitude above four metasurfaces containing square Si pillars placed on a 200 nm square lattice under illumination at $\lambda_0 = 1550$ nm, with the electric field polarized in the plane of the figure. (a) $f = 50\%$, traditional ARC approach (b) $f = 50\%$ with ARC optimized for $f = 50\%$, (c) $f = 75\%$, and traditional ARC approach (d) $f = 75\%$ with ARC optimized for $f = 75\%$.

with $\lambda_0 = 1550$ nm for a meta-atom size of L = 200 nm. The 2D cut is taken through the center of the Si pillars, and the electric field is polarized along the x-direction. Figures 3(a) and 3(b) show the traditional and optimized ARC for a Si fill fraction of $f = 0.5$. Note the significantly larger layer thickness required to achieve optimum performance at $f = 0.5$. The standard approach is seen to produce a clearly visible standing wave pattern above the surface, which is almost entirely eliminated when using the optimized approach. Figures 3(c) and 3(d) show the equivalent graphs for $f = 0.75$. The thickness difference between the two approaches is not as striking in this case; however, again a substantial standing wave pattern is observed when using the traditional ARC approach [Fig. 3(c)], which is again almost entirely eliminated when using the optimized ARC structure [Fig. 3(d)]. The demonstrated drastic reduction of surface reflections from high-index metasurfaces is expected to allow for significantly reduced image artifacts and ghost images in metasurface optics-based imaging systems, representing a substantial practical improvement in real-world applications of metalenses and related structures.

In summary, we have studied the suppression of surface reflections in high-index gradient metasurface structures using optimized anti-reflection coatings. Theoretical predictions of the optimum ARC material index and thickness were made, and predictions based on effective medium theory were borne out by calculations based on the RCWA method. It was shown that anti-reflective coatings optimized for a fill fraction of 50% outperform the traditional approach by over a factor of 5 for Si-based metasurfaces with areal fill fractions up to 73%. In addition, reflectance values below 0.5% could be obtained for areal fill fractions below 88% using an ARC optimized for a fill fraction of 75%. This work shows a path toward low-reflection metasurface optics, with an approach that is compatible with standard 2D fabrication methods involving a single patterning step.

See the supplementary material for the derivation of Eq. (1).

This work was supported by NSF Grant No. ECCS-1650002.

AUTHOR DECLARATIONS

Conflict of Interest

The authors have no conflicts to disclose.

Author Contributions

Mengdi Sun: Investigation (equal); Writing – original draft (lead); Writing – review & editing (equal). **Pieter G. Kik:** Funding acquisition (lead); Investigation (equal); Writing – review & editing (equal).

DATA AVAILABILITY

The data that support the findings of this study are available from the corresponding author upon reasonable request.

REFERENCES

[1] Editorial, Nat. Photonics **17**(1), 1 (2023).
[2] G. Pitruzzello, Nat. Photonics **17**(1), 6 (2023).
[3] D. N. Neshev and A. E. Miroshnichenko, Nat. Photonics **17**(1), 26 (2023).
[4] Y. Wang, P. Landreman, D. Schoen, K. Okabe, A. Marshall, U. Celano, H. S. Philip Wong, J. Park, and M. L. Brongersma, Nat. Nanotechnol. **16**(6), 667 (2021).
[5] P. C. Wu, R. Sokhoyan, G. Kafaie Shirmanesh, W.-H. Cheng, and H. A. Atwater, Adv. Opt. Mater. **9**(16), 2100230 (2021).
[6] H. Pahlevaninezhad, M. Khorasaninejad, Y.-W. Huang, Z. Shi, L. P. Hariri, D. C. Adams, V. Ding, A. Zhu, C.-W. Qiu, F. Capasso, and M. J. Suter, Nat. Photonics **12**(9), 540 (2018).
[7] Q. Guo, Z. Shi, Y.-W. Huang, E. Alexander, C.-W. Qiu, F. Capasso, and T. Zickler, Proc. Natl. Acad. Sci. U. S. A. **116**(46), 22959 (2019).
[8] A. L. Holsteen, D. Lin, I. Kauvar, G. Wetzstein, and M. L. Brongersma, Nano Lett. **19**(4), 2267 (2019).
[9] C. Schlickriede, N. Waterman, B. Reineke, P. Georgi, G. Li, S. Zhang, and T. Zentgraf, Adv. Mater. **30**(8), 1703843 (2018).
[10] E. Schonbrun, K. Seo, and K. B. Crozier, Nano Lett. **11**(10), 4299 (2011).
[11] H. Zuo, D.-Y. Choi, X. Gai, P. Ma, L. Xu, D. N. Neshev, B. Zhang, and B. Luther-Davies, Adv. Opt. Mater. **5**(23), 1700585 (2017).
[12] K. Shastri and F. Monticone, Nat. Photonics **17**(1), 36 (2023).
[13] K. Wang, M. Chekhova, and Y. Kivshar, Phys. Today **75**(8), 38 (2022).
[14] S. M. Kamali, E. Arbabi, A. Arbabi, Y. Horie, M. Faraji-Dana, and A. Faraon, Phys. Rev. X **7**(4), 041056 (2017).
[15] G.-Y. Lee, J.-Y. Hong, S. Hwang, S. Moon, H. Kang, S. Jeon, H. Kim, J.-H. Jeong, and B. Lee, Nat. Commun. **9**(1), 4562 (2018).
[16] W.-J. Joo and M. L. Brongersma, Science **377**(6613), 1376 (2022).
[17] S. M. Kamali, E. Arbabi, A. Arbabi, Y. Horie, and A. Faraon, "Highly tunable elastic dielectric metasurface lenses," Laser Photonics Rev. **10**, 1002–1008 (2016).
[18] M. G. Moharam and T. K. Gaylord, J. Opt. Soc. Am. **71**(7), 811 (1981).
[19] J.-P. Hugonin and P. Lalanne (2021). "Light-in-complex-nanostructures/RETICOLO: V9 (Version 9a)," Zenodo. https://doi.org/10.5281/zenodo.5905381
[20] H. Kikuta, Y. Ohira, H. Kubo, and K. Iwata, J. Opt. Soc. Am. A **15**(6), 1577 (1998).